Talanta 219 (2020) 121209

Contents lists available at ScienceDirect

Talanta

journal homepage: www.elsevier.com/locate/talanta

Dendrimer grafted persistent luminescent nanoplatform for aptamer guided tumor imaging and acid-responsive drug delivery

Hong-Jiao Zhang[a], Xu Zhao[b,c,d], Li-Jian Chen[b,c,d], Cheng-Xiong Yang[a], Xiu-Ping Yan[b,c,d,*]

[a] Research Center for Analytical Sciences, Tianjin Key Laboratory of Molecular Recognition and Biosensing, College of Chemistry, Nankai University, Tianjin, 300071, China
[b] State Key Laboratory of Food Science and Technology, Jiangnan University, Wuxi, 214122, China
[c] International Joint Laboratory on Food Safety, Jiangnan University, Wuxi, 214122, China
[d] Institute of Analytical Food Safety, School of Food Science and Technology, Jiangnan University, Wuxi, 214122, China

ARTICLE INFO

Keywords:
Theranostics
Persistent luminescence
Bioimaging
Dendrimer
Drug delivery

ABSTRACT

Theranostic nano-drug delivery systems are promising candidates for early diagnosis and treatment of tumors. However, it is a great challenge to achieve accurate intracellular delivery and stimuli-responsive drug release with the enhanced anti-tumor effects and reduced side effects. Herein we report the fabrication of polyamide-amine (PAMAM) dendrimer grafted persistent luminescence nanoparticles (PLNPs) via in situ growth of PAMAM on the surface of PLNPs and its application in targeted bioimaging and drug delivery. The developed PLNPs-PAMAM possesses strong renewable near-infrared persistent luminescence for imaging and gives abundant terminal groups for further functionalization. Aptamer AS1411 coupled to the PLNPs-PAMAM surface can specifically bind to the over-expressed nucleolin on the membrane of tumor cells and improve the intracellular accumulation of the nanoparticles. Doxorubicin (DOX) is loaded on PLNPs-PAMAM by a pH-sensitive hydrazine, can be specifically released in the intracellular acid environment, leading to apoptosis of HeLa tumor cells and inhibition of tumor growth. The as-prepared smart drug delivery nanoplatform with persistent luminescence, PLNPs-PAMAM-AS1411/DOX, shows a good application prospect for precise cancer theranostics.

1. Introduction

Cancer is a disease with high incidence rate and high mortality rate, and has seriously threatened human health [1,2]. The emergence and development of chemotherapeutic agents delivery system mediated by nanoparticles have brought opportunities to overcome the shortcomings of traditional chemotherapy drugs with nonspecific distribution, systemic toxicity and poor therapeutic effect [3,4]. The multifunctional intelligent drug delivery systems based on various nanoparticles with special properties such as optical imaging, photothermal and photodynamic therapy have gained considerable attention [5–7]. Persistent luminescence nanoparticles (PLNPs) can release afterglow signal slowly for a long time after stopping excitation, and have aroused widespread interest for autofluorescence free bioimaging because of their unique optical properties such as no need for in-situ excitation, near infrared (NIR) luminescence and persistent luminescent renewability by NIR light [8–11]. These unique properties have paved the way to biomedical applications [9].

Previous PLNPs-based theranostic drug delivery systems have been developed by encapsulating other materials (mesoporous silica [12], hollow silica [13], liposomes [14] and zeolitic imidazolate framework-8 [15]) with drug loading capability. Dendrimers, a class of fully branched polymers consisting of a series of repetitive units extending outward from the core, have aroused wide attention in recent years because of their precise molecular structure, high geometric symmetry and controllable molecular weight [16–18]. Dendrimers can endow nanoparticles with abundant superficial functional groups compared with other polymers, which is of great significance to improve surface properties and new functions [19–21]. Polyamide-amine (PAMAM) dendrimer is simple to prepare and possesses good physical and chemical properties, and has played a role in biomedical applications such as drug delivery [22–28].

Targeted intracellular delivery and stimuli-responsive release are crucial for nano-drug delivery system to enhance theranostic efficiency. Compared with conventional passive targeting from the enhanced permeation and retention (EPR) effect in the tumor vasculature, active targeting strategy via specific binding of ligands to tumor markers greatly improves intracellular accumulation. The targeting ligands

* Corresponding author. State Key Laboratory of Food Science and Technology, Jiangnan University, Wuxi, 214122, China.
E-mail address: xpyan@jiangnan.edu.cn (X.-P. Yan).

https://doi.org/10.1016/j.talanta.2020.121209
Received 24 April 2020; Received in revised form 20 May 2020; Accepted 21 May 2020
Available online 26 May 2020
0039-9140/

including folic acid [29], RGD peptide [30], phenylboronic acid [31] and galactose [32] are often coupled to the surface of nanoparticles to perform active targeting functions. Aptamers are considered excellent candidates for targeting tumors due to their ability to bind specifically to target molecules with high affinity [33,34]. Various aptamers such as AS1411 [35] and MUC1 [36] have been coupled to the surface of drug delivery systems to increase their ability to enter cancer cells. In addition, conjugating drug candidates to the surface of nanocarriers via specific linkers such as pH-sensitive covalent bonds and enzyme-cleavable peptide that can be broken in cancer cells upon microenvironment stimulation is an effective strategy to achieve controlled drug release with a slight side effect [37–42].

Herein, we report the preparation of PAMAM grafted PLNPs (PLNPs-PAMAM) with terminal hydrazide group as the nanoplatform for aptamer guided imaging and acid-responsive drug delivery. PLNPs is used as the core of the nanoplatform due to its super long NIR persistent luminescence. PAMAM is grafted onto the surface of PLNPs to improve the biocompatibility of the nanoplatform and to provide abundant terminal groups for further functionalization and drug loading. Further conjugation of aptamer AS1411 endows the nanoplatform with targeting ability with high specificity for the over-expressed nucleolin on the membrane of cancer cells.

2. Experimental section

2.1. Preparation of PLNPs-PAMAM

The PLNPs and amino-functionalized PLNPs (PLNPs-NH_2) were prepared according to our previous work [11]. The 2.5th generation (G2.5) PAMAM dendrimer grafted PLNPs was first synthesized with ester end-functional groups [43]. Briefly, 250 mg of PLNPs-NH_2 was dispersed in 12.5 mL methanol, then 2.5 mL methyl acrylate (MA) was added under stirring. After 2-day reaction, the resulting the half generation PLNPs-PAMAM (G0.5) was collected by centrifugation, washed and re-dispersed in 12.5 mL methanol. To the PLNPs-PAMAM (G0.5) methanol dispersion, 12.5 mL ethylenediamine (EDA) was added under stirring. After another 2 d reaction, the product PLNPs-PAMAM (G1) was separated by centrifugation and washed with methanol. G1.5, G2 and G2.5 were acquired by repeating the above two steps. Furthermore, the third generation (G3) PAMAM dendrimer grafted PLNPs with hydrazide end-functional groups was obtained from the reaction of PLNPs-PAMAM G2.5 with hydrazine hydrate as described above.

2.2. Conjugation of aptamer AS1411

AS1411 was conjugated onto the surface of PLNPs-PAMAM (G3) via an amide condensation reaction. 15 μL of AS1411 (100 μM) was mixed with 900 μL phosphate buffer solution (PBS, pH 7.4) containing 100 μL 1-ethyl-3-(3-dimethylaminopropyl) carbodiimide hydrochloride (EDC) (100 mg mL^{-1}) and *N*-hydroxysuccinimide (NHS) (100 mg mL^{-1}) under stirring. After activation for 15 min, 100 μL of PLNPs-PAMAM (5 mg mL^{-1}) was added to the mixture solution. After 12-h reaction, the resulting PLNPs-PAMAM-AS1411 was collected by centrifugation, washed and dried for further use.

2.3. Loading of DOX

The PLNPs-PAMAM-AS1411/DOX nanoplatform was prepared by coupling DOX to PLNPs-PAMAM-AS1411 via an acylhydrazone bond. Briefly, 0.5 mg PLNPs-PAMAM-AS1411 and 0.25 mg DOX were mixed in 100 μL dimethyl sulfoxide (DMSO), and then a few drops of acetic acid were added as catalyst. After 48 h stirring reaction in dark, the resulting PLNPs-PAMAM-AS1411/DOX was collected by centrifugation, washed and dried. In addition, the PLNPs-PAMAM-DOX was prepared in the same way.

2.4. Hydrolytic release of DOX

The *in vitro* release of DOX from PLNPs-PAMAM-AS1411/DOX was assessed via dialysis. The prepared PLNPs-PAMAM-AS1411/DOX was separately dispersed in PBS solution at pH 7.4 and 5.0, transferred into a dialysis bag and placed in PBS solution under constant shaking. At the designed time points, 1 mL of release medium was taken out for the measurement of DOX and 1 mL fresh PBS was added again for further drug release. The DOX released were determined by fluorescence spectrometry at 600 nm.

2.5. Cell imaging

HeLa and 3T3 cell lines (Shanghai cell bank of Chinese Academy of Sciences) were cultured in DMEM medium, and seeded into the confocal dish with 5×10^3/well in incubator at 37 °C in 5% CO_2. After 24 h culture, the medium was replaced with the fresh medium containing 50 μg mL^{-1} of PLNPs-PAMAM-AS1411/DOX, and incubated for additional 2 h. Afterwards, the medium was removed and the cell was immobilized using 4% polyformaldehyde for 15 min. The cell imaging was performed on confocal laser scanning microscopy (CLSM) after staining with DAPI solution for 10 min. The DOX release behavior of PLNPs-PAMAM-AS1411/DOX in HeLa cell was explored as described above.

2.6. Flow cytometry

HeLa and 3T3 cells were seeded in a 6-well with a density of 1×10^4/well and cultured for 24 h. Further incubation was carried out using a fresh medium containing 50 μg mL^{-1} PLNPs-PAMAM-AS1411/DOX for 2 h. The medium was then discarded and the cells were washed with PBS for three times, digested with 0.25% trypsin, collected by centrifugation for flow cytometry analysis.

2.7. MTT assay

To evaluate the cytotoxicity of PLNPs-PAMAM-AS1411 and the chemotherapeutic efficacy of PLNPs-PAMAM-DOX and PLNPs-PAMAM-AS1411/DOX, HeLa and 3T3 cells were planted into the 96-well plates (1×10^4 cells/well) and cultured for 24 h. Then, the medium was replaced with a fresh medium containing different concentrations (0, 10, 30, 60 and 100 μg mL^{-1}) of PLNPs-PAMAM-AS1411. Continuous incubation was carried out with a fresh medium containing 0.25 mg mL^{-1} MTT for 4 h. The DMSO (100 μL/well) was added to dissolve the MTT-formazan produced by living cells after removing the old medium. At last, the cell viability was calculated according to the measured absorbance values at 490 nm via a microplate reader.

The viability of HeLa cells in media containing different concentrations (0, 0.1, 0.5, 1, 2, 3 and 5 μg mL^{-1} as DOX) of free DOX, PLNPs-PAMAM-DOX and PLNPs-PAMAM-AS1411/DOX was examined with 4-h incubation in accordance with the above procedure, respectively. The absorption was determined after a further incubation for 36 and 72 h.

2.8. In vivo imaging of HeLa tumor-bearing mice

Animal experiments strictly followed the guidelines of the Tianjin Committee of Use and Care of Laboratory Animals, and approved by the Animal Ethics Committee of Nankai University. The Balb/c nude mice (4 weeks, female, 15 g) were purchased from Shanghai Slac laboratory animal Co, Ltd. HeLa cells (5×10^6 cells per mouse) were inoculated into nude mice by subcutaneous injection to produce tumors.

The PLNPs-PAMAM-DOX and PLNPs-PAMAM-AS1411/DOX (200 μL, 2 mg mL^{-1} as PLNPs) after a pre-excitation with a 254 nm UV light for 10 min were injected into mice via tail vein. Repeated activations were carried out by irradiating mice with a LED lamp (650 ± 10 nm, 5000 lm) for 2 min before acquiring images. The

persistent luminescence signals were collected on the IVIS Imaging System at designed time points.

2.9. In vivo therapeutic effect

HeLa tumor-bearing mice were randomly assigned to 4 groups and then intravenously injected with PBS, free DOX, PLNPs-PAMAM-DOX and PLNPs-PAMAM-AS1411/DOX (200 μL, 0.3 mg mL^{-1} as DOX) once every two days for three times, respectively. The length and width of the tumor were measured every two days for 20 days and the volumes were calculated by the formula: length × $width^2/2$ for ellipsoid tumors [44,45]. The body weight changes of mice were recorded during treatment.

2.10. Statistical analysis

Experimental data are expressed as means ± standard deviation. Significance analysis was carried out by two-way ANOVA.

3. Results and discussion

3.1. Design, preparation and characterisation of PLNPs-PAMAM-AS1411/DOX

The design and preparation of PLNPs-PAMAM-AS1411/DOX theranostic nanoplatform for aptamer guided persistent luminescence imaging and acid-responsive drug delivery are illustrated in Scheme 1. To grow PAMAM dendrimer on the surface of the PLNPs, PLNPs-NH_2 was prepared according to our previous work [11]. The propagation of PAMAM dendrimer onto the surface of PLNPs-NH_2 was performed via a standard method for synthesizing PAMAM dendrimer. MA reacted first with the amine groups of PLNPs-NH_2 via Michael addition reaction to form PLNPs-PAMAM (G0.5). Subsequent amidation of EDA and the prepared G0.5 gave the first generation of PLNPs-PAMAM (G1). Other generations of PLNPs-PAMAM (G1.5, G2 and G2.5) were prepared by repeating the steps described above. The third generation of PLNPs-PAMAM (G3) with hydrazine group as terminal group was obtained by an amidation of hydrazine hydrate. Such grafting of PAMAM dendrimer on the surface of PLNPs provides abundant active groups for drug loading and improves the water solubility of the nanoparticles. Subsequently, the aptamer AS1411 was conjugated onto the surface of PLNPs-PAMAM (G3) via amide condensation to give the nanoplatform the ability to target cancer cells. Finally, DOX was loaded onto the nanoplatform via acid-sensitive hydrazone bond to achieve intracellular response release of drugs.

The as-synthesized PLNPs were spherical nanoparticles with an average size of 15.2 nm (calculated from 100 randomly selected particles) (Figs. S1a and b) as well as the spinel phase of Zn_2GeO_4 (JCPDS 25–1018) and $ZnGa_2O_4$ (JCPDS 38–1240) (Fig. S1c) and the lattice space of 0.272 nm (Fig. S1d). TEM images also reveal that the morphology and size of the nanoparticles did not change significantly after grafting PAMAM (Fig. 1 a-f. Figs. S1a and b).

The successful preparation of PLNPs-PAMAM was confirmed by FT-IR spectrometry (Fig. 2a). The PLNPs-NH_2 gave N–H bending vibrations from –NH_2 at 1632 cm^{-1}, strong stretching vibrations of O–Si–O at 1042 and 1122 cm^{-1}, and the symmetrical and asymmetrical stretching vibrations of –CH_2- at 2925 and 2855 cm^{-1}, suggesting the successful amino functionalization. All half-generation products including G0.5, G1.5 and G2.5 showed clear stretching vibration bands of C═O from the ester groups at 1737 cm^{-1}, indicating that MA reacted with the amino groups on the surface of PLNPs-NH_2 and the propagation occurred. However, the above ester band disappeared in the FT-IR spectra of the corresponding full-generation products (G1, G2, and the hydrazine hydrate of G3 (PLNPs-PAMAM-hyd)), demonstrating successful amidation with EDA. Moreover, the FT-IR spectra of the products starting from the first generation display the strong bands from the C═O stretching of –CONH– at 1651 and 1560 cm^{-1}.

Growth of PAMAM with subsequent conjugation of the aptamer AS1411 onto the surface of PLNPs-NH_2 was also evidenced by the changes of the Zeta potential and the hydrodynamic size. Zeta potential of PLNPs-NH_2 is 21.4 mV and that of PLNPs-PAMAM (G1, G2 and G3) slightly increased as the increase of grafting generation due to the increase of amino groups on the surface of nanoparticles (Fig. 2b). The conjugating of aptamer AS1411 made the Zeta potential dramatically decreased to −7.0 mV owing to the negative charge of the phosphoric acid skeleton in the aptamer. Furthermore, the hydrodynamic size of the increased from 58.1 nm for PLNPs-NH_2 to 110.3 nm for PLNPs-PAMAM-AS1411 due to the introduction of PAMAM and aptamer AS1411 (Fig. 2c).

Elemental mapping further confirms the successful synthesis of PLNPs-PAMAM-AS1411. While Zn and Ga represent the PLNPs core, C and N are mainly from PAMAM and AS1411, and P comes from the phosphoric acid skeleton of AS1411 (Fig. 2d). PLNPs-PAMAM-AS1411/DOX gave the characteristic absorption band at 490 nm (Fig. S2a) and the fluorescence emission at 600 nm (Fig. S2b), demonstrating the successful loading of DOX.

3.2. Persistent luminescence performance

The as-prepared PLNPs gave a near infrared luminescence emission at 700 nm originating from the $^2E \rightarrow {}^4A2$ transition of distorted Cr^{3+} ions in gallogermanate with an excitation spectra in the ultraviolet region (Fig. 3a; Figs. S3a and b), and exhibited good persistent luminescence performance after stopping excitation with a 254 nm ultraviolet lamp for 5 min (Fig. S4a). Furthermore, the persistent luminescence can be repeatedly activated via a 650 nm red LED lamp (Fig. S4b and Fig. S5). PLNPs-PAMAM-AS1411/DOX had similar luminescent and afterglow properties (Fig. 3a and b).

3.3. Targeted cellular uptake

To examine the targeted cellular uptake and imaging performance of PLNPs-PAMAM-AS1411/DOX, HeLa (cancer cells, overexpressed nucleolin) and 3T3 (normal cells, low nucleolin expression) were selected as model cells. CLSM imaging and flow cytometry analysis show much stronger luminescence signal (red) of the PLNPs in the cytoplasm of HeLa cells compared to 3T3 cells after incubation with PLNPs-PAMAM-AS1411/DOX (Fig. 4a–c), indicating that the specific binding of AS1411 and over-expressed nucleolin on the membrane of HeLa cells promoted the uptake of PLNPs-PAMAM-AS1411/DOX. To further confirm that the targeting effect originates from aptamer AS1411, the inhibition experiment was carried out by adding aptamer AS1411 in advance. As expected, the luminescence intensity dramatically decreased for HeLa cell because the added AS1411 blocked the affinity interaction between PLNPs-PAMAM-AS1411/DOX and the nucleolin, but did not show obvious change for 3T3 cells (Fig. 4 a,d,e).

In addition, the influence of incubation time on the uptake capacity of HeLa and 3T3 cells was investigated. HeLa cells showed high uptake efficiency due to the active targeting of the PLNPs-PAMAM-AS1411/DOX to HeLa cells and the uptake approached to the maximum within 3 h (Figs. S6a and b). In contrast, 3T3 cells exhibited much lower uptake efficiency in a strong time dependent manner and the uptake increased slowly with incubation time (Figs. S6c and d).

3.4. DOX loading and release

The influence of DOX content in the reaction system and different generations of PLNPs-PAMAM (G1, G2 and G3) with hydrazide as the terminal on DOX loading capacity was investigated. The DOX loading capacity increased rapidly with the added amount of DOX below 2.0 mg mg^{-1}, then tended to the maximum because the reaction sites gradually exhausted (Fig. S7). In addition, the DOX loading capacity

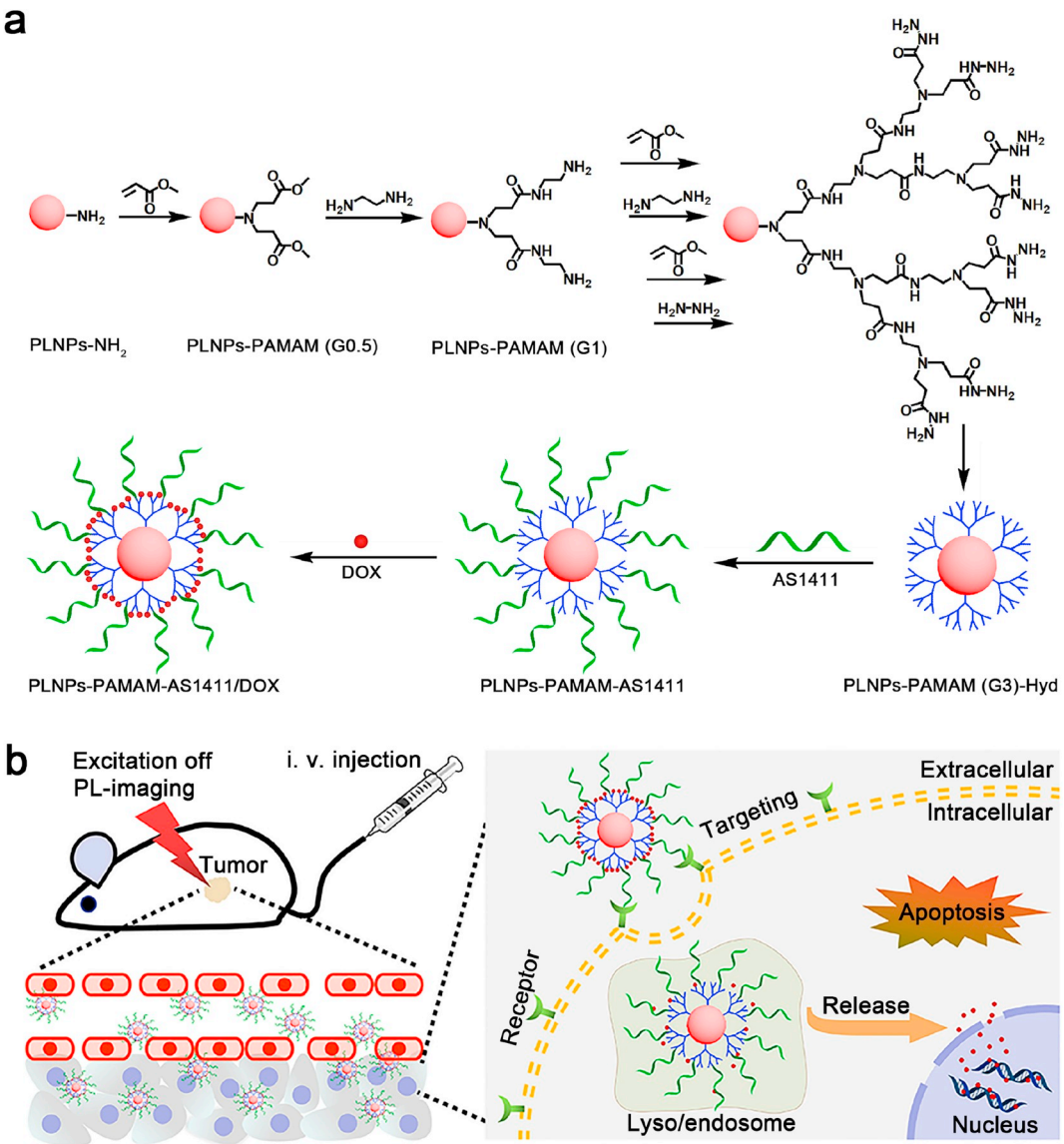

Scheme 1. (a) Scheme for the synthesis of PLNPs-PAMAM-AS1411/DOX. (b) Illustration for the utilization of PLNPs-PAMAM-AS1411/DOX as the nanoplatform for aptamer AS1411 guided tumor imaging and acid-responsive drug delivery.

increased with the increase of grafting generation due to the production of more reaction sites on the surface of the nanoprobe (Fig. S8). This fully reflects the necessity of introducing dendrimers to effectively improve drug loading.

We then examined the acid-responsive DOX release performance of PLNPs-PAMAM-DOX or PLNPs-PAMAM-AS1411/DOX nanocomposites. Buffer solutions at pH 7.4 (normal physiological environment) and pH 5.0 (acidic cellular compartments (endosome/lysosome)) were chosen as simulation systems. The DOX release from PLNPs-PAMAM-DOX and PLNPs-PAMAM-AS1411/DOX at pH 5.0 was significantly faster than that at pH 7.4 (Fig. 5a). More than 60% of DOX released at pH 5.0 in 36 h, whereas only about 10% of DOX released at pH 7.4. Such a remarkable difference indicates that the PLNPs-PAMAM-DOX and PLNPs-PAMAM-AS1411/DOX nanocomposites possess excellent acid-responsive ability to achieve controlled drug release, leading to high drug utilization and low side effects, which is conducive to the application in cancer therapy. This specific response is attributed to the acid sensitivity of the hydrazone bond between DOX molecules and PLNPs-PAMAM which is stable under neutral condition but cleavable due to hydrolysis under acidic condition (Fig. 5b).

The intracellular release of DOX from PLNPs-PAMAM-AS1411/DOX was further demonstrated on HeLa cells (Fig. 5c). CLSM imaging of the cells after 1 h incubation with the nanoprobe shows the luminescence signal (red) of DOX from PLNPs-PAMAM-AS1411/DOX nanocomposites mainly appeared in cytoplasm, indicating that only a small amount of the DOX released within 1 h. In contrast, free DOX displayed strong luminescence signal in the nucleus of HeLa cells because DOX is a water-soluble small molecule and can quickly spread to the cells and intercalate DNA in the nucleus [18]. The luminescence signal of DOX from PLNPs-PAMAM-AS1411/DOX was significant in the nucleus after 5 h incubation as the DOX gradually released in an acid intracellular environment (endosome/lysosome) of HeLa cells.

3.5. *In vivo* persistent luminescence imaging

The performance of *in vivo* persistent luminescence imaging of PLNPs-PAMAM-AS1411/DOX was investigated by subcutaneous injection on normal nude mice. The persistent luminescence imaging signal can be observed after stopping excitation, and the persistent luminescence intensity can be restored quickly and effectively after repeated activations with LED lamp (Fig. S9). *In vivo* imaging after subcutaneous injection of PLNPs-PAMAM-AS1411/DOX and DOX was carried out for

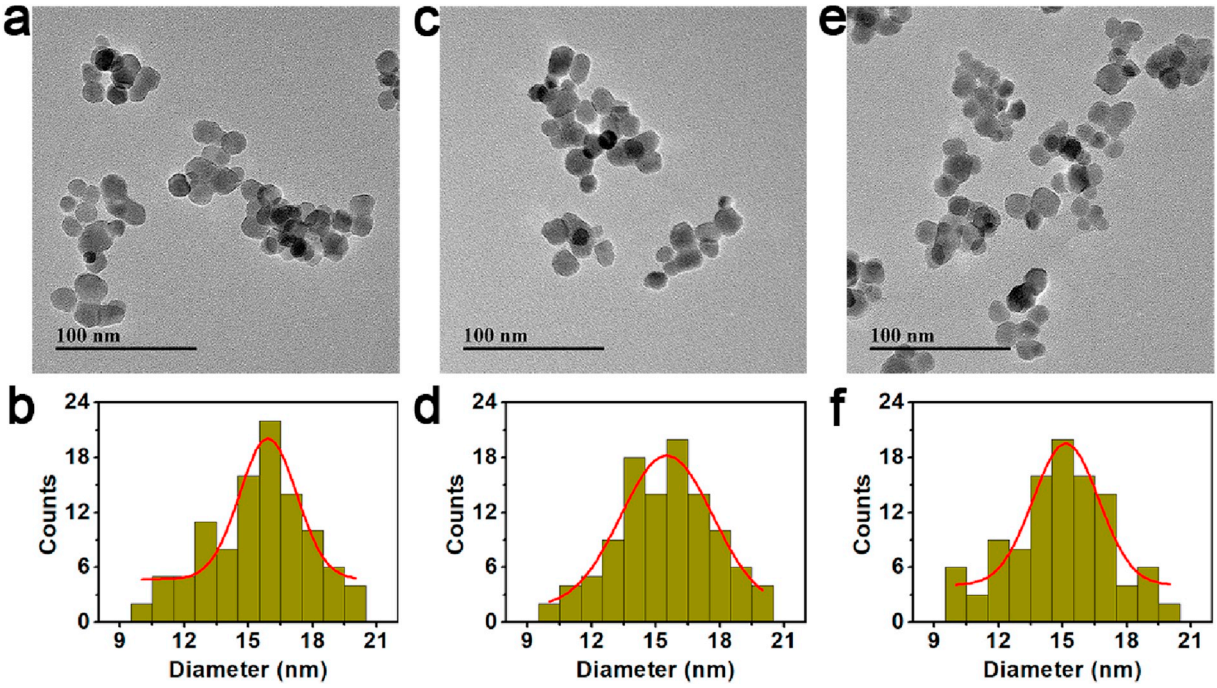

Fig. 1. TEM images (a,c,e) and diameter distributions (b,d,f) of PLNPs-PAMAM (G1) (a,b), PLNPs-PAMAM (G2) (c,d), PLNPs-PAMAM (G3) (e,f).

comparison (Fig. 6). The signal-to-noise ratio (SNR) of PLNPs-PAMAM-AS1411/DOX (227) was much higher than that of the DOX (2.96) due to the absence of autofluorescence interference under the condition of no in situ excitation for PLNPs-PAMAM-AS1411/DOX. In addition, the ventral views of mice show that the PLNPs-PAMAM-AS1411/DOX can still give clear persistent luminescence imaging signal with a strong tissue penetration from the near-infrared luminescence, while the DOX cannot provide a resolvable fluorescence imaging signal. These excellent properties of PLNPs-PAMAM-AS1411/DOX pave the way to its application *in vivo* autofluorescence-free imaging.

The inspiring results of the *in vitro* cell targeted uptake and *in vivo* imaging encouraged us to evaluate PLNPs-PAMAM-AS1411/DOX for *in vivo* target-specific cancer imaging. PLNPs-PAMAM-DOX was used for comparison. PLNPs-PAMAM-DOX and PLNPs-PAMAM-AS1411/DOX were irradiated with a 254 nm UV light for 10 min before injection. 2 min LED light (650 nm) irradiation was applied on the mice before acquisiting luminescence images. Significant luminescence signal from PLNPs-PAMAM-AS1411/DOX was observed in the tumor area of HeLa tumor-bearing mice for at least 8 h (Fig. 7a), while the PLNPs-PAMAM-DOX doesn't give a visual image signal, indicating that AS1411 aptamer

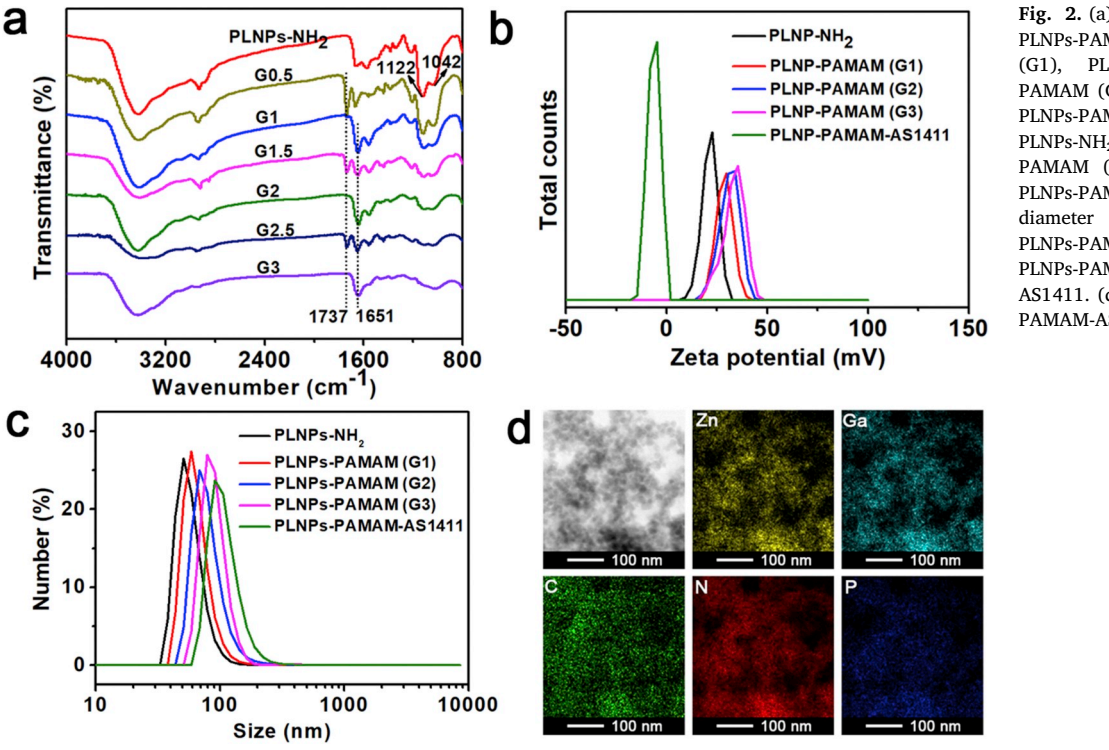

Fig. 2. (a) FT-IR spectra of PLNPs-NH_2, PLNPs-PAMAM (G0.5), PLNPs-PAMAM (G1), PLNPs-PAMAM (G1.5), PLNPs-PAMAM (G2), PLNPs-PAMAM (G2.5), and PLNPs-PAMAM (G3). (b) Zeta potentials of PLNPs-NH_2, PLNPs-PAMAM (G1), PLNPs-PAMAM (G2), PLNPs-PAMAM (G3) and PLNPs-PAMAM-AS1411. (c) Hydrodynamic diameter distributions of PLNPs-NH_2, PLNPs-PAMAM (G1), PLNPs-PAMAM (G2), PLNPs-PAMAM (G3) and PLNPs-PAMAM-AS1411. (d) Elemental mapping of PLNPs-PAMAM-AS1411.

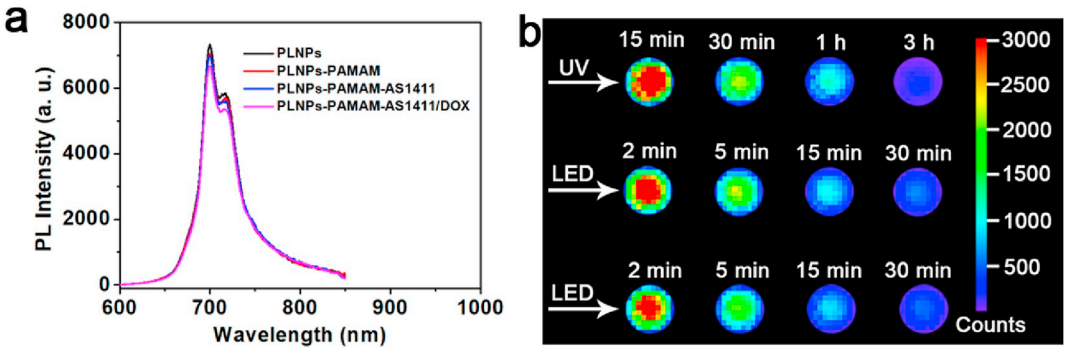

Fig. 3. (a) Emission spectra of the PLNPs, PLNPs-PAMAM, PLNPs-PAMAM-AS1411 and PLNPs-PAMAM-AS1411/DOX. (b) Persistent luminescence images of the PLNPs-PAMAM-AS1411/DOX aqueous dispersion after 5 min excitation with a 254 nm UV lamp and 2 min re-activation with red LED light. (For interpretation of the references to colour in this figure legend, the reader is referred to the Web version of this article.)

functionalized nanoprobe has active targeting effect and can promote the accumulation of nanoparticle in tumor site. In addition, the major persistent luminescence signal appeared in the liver area (one of the major reticuloendothelial system organs) because of the strong phagocytosis. Furthermore, the concentrations of element Ga from PLNPs 8 h and 24 h after intravenous injection further revealed the distribution of PLNPs-PAMAM-DOX and PLNPs-PAMAM-AS1411/DOX in the major organs (heart, liver, spleen, lung and kidney) and tumors (Fig. 7b). The uptake of the nanoprobes by HeLa tumor increased with time, while the accumulation of PLNPs-PAMAM-AS1411/DOX in tumor area is significantly higher than that of PLNPs-PAMAM-DOX.

3.6. Toxicity evaluation of PLNPs-PAMAM-AS1411

In vitro cytotoxic evaluation of PLNPs-PAMAM-AS1411 against cancer cell HeLa and normal cell 3T3 was carried out by MTT assay. No noticeable toxicity to the two cell lines was observed after incubation with PLNPs-PAMAM-AS1411 at concentrations ranging from 0 to 100 μg mL^{-1} for 24 h (Fig. S10). For further assessment of *in vivo* toxicity, the nude mice were divided into one control group without any treatment and one experimental group injected intravenously with PLNPs-PAMAM-AS1411. The mice viability was still 100% at 20 days after tail vein injection of PLNPs-PAMAM-AS1411 and the weight gain of the PLNPs-PAMAM-AS1411 treated group and the control group of the mice exhibited a similar trend (Fig. S11). In addition, the histological examination revealed that the main organs (heart, liver, spleen, lung and kidney) of PLNPs-PAMAM-AS1411 treated group had no appreciable damage sign or abnormality compared with the control group (Fig. S12). The above results demonstrate that PLNPs-PAMAM-AS1411 possesses good biocompatibility for biomedical application.

3.7. In vitro anti-tumor activity

The cytotoxicity of free DOX, PLNPs-PAMAM-DOX and PLNPs-PAMAM-AS1411/DOX towards HeLa cells were tested by MTT assay to evaluate anticancer activity (Fig. 8a and b). Overall, the lethal effects of free DOX, PLNPs-PAMAM-DOX and PLNPs-PAMAM-AS1411/DOX on cells were positively correlated with incubation time and DOX concentration. The concentration yielding half-lethal (LC50) to HeLa cell was tested as 1.9, 2.3 and 3.6 μg mL^{-1} (as DOX) for free DOX, PLNPs-PAMAM-AS1411/DOX and PLNPs-PAMAM-DOX. The cytotoxicity of PLNPs-PAMAM-AS1411/DOX with targeting effect for nucleolin was higher than that of PLNPs-PAMAM-DOX, which is also consistent with the results observed in confocal imaging of cell uptake and drug release.

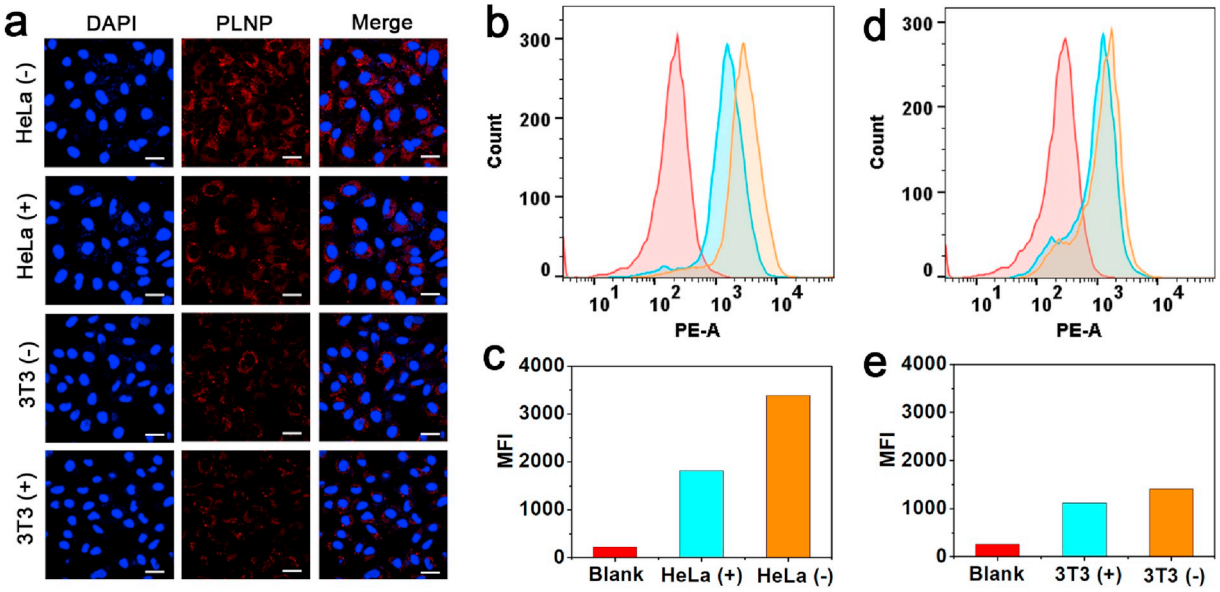

Fig. 4. (a) CLSM images of HeLa and 3T3 cells incubated with PLNPs-PAMAM-AS1411/DOX (−) and PLNPs-PAMAM-AS1411/DOX (+) for 2 h + and - represent with and without inhibition from the aptamer AS1411, respectively. Flow cytometry analysis and the corresponding mean luminescence intensity (MFI) of HeLa (b,c) and 3T3 (d,e) cells treated with PLNPs-PAMAM-AS1411/DOX (−) and PLNPs-PAMAM-AS1411/DOX (+) for 2 h.

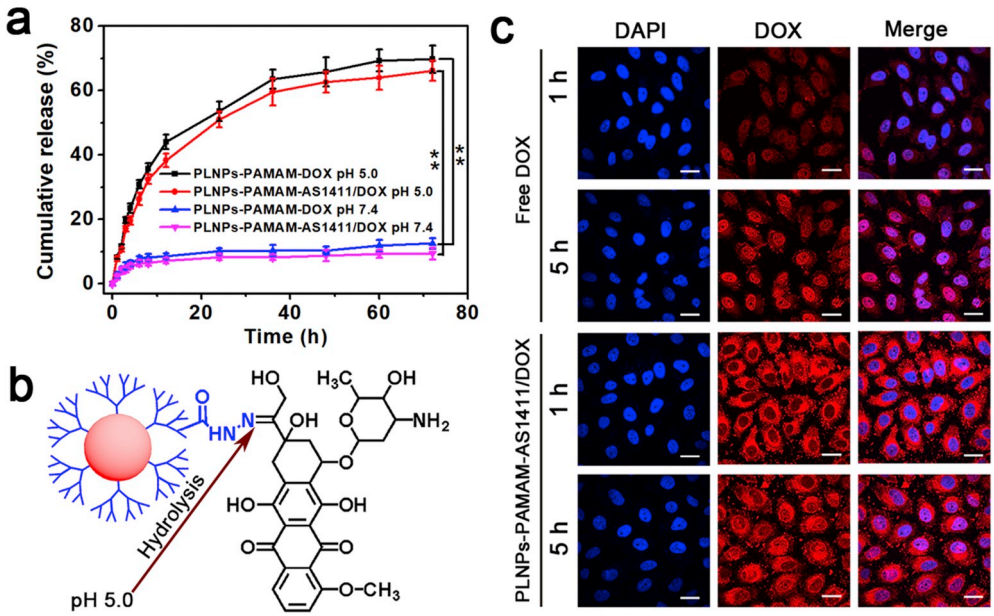

Fig. 5. (a) Release profiles of DOX from PLNPs-PAMAM-DOX and PLNPs-PAMAM-AS1411/DOX in neutral (pH 7.4) and acidic (pH 5.0) media. (b) Illustration of acid-responsive DOX release mechanism. (c) CLSM images of HeLa cells treated with free DOX and PLNPs-PAMAM-AS1411/DOX for 1 and 5 h (scale bar, 30 μm).

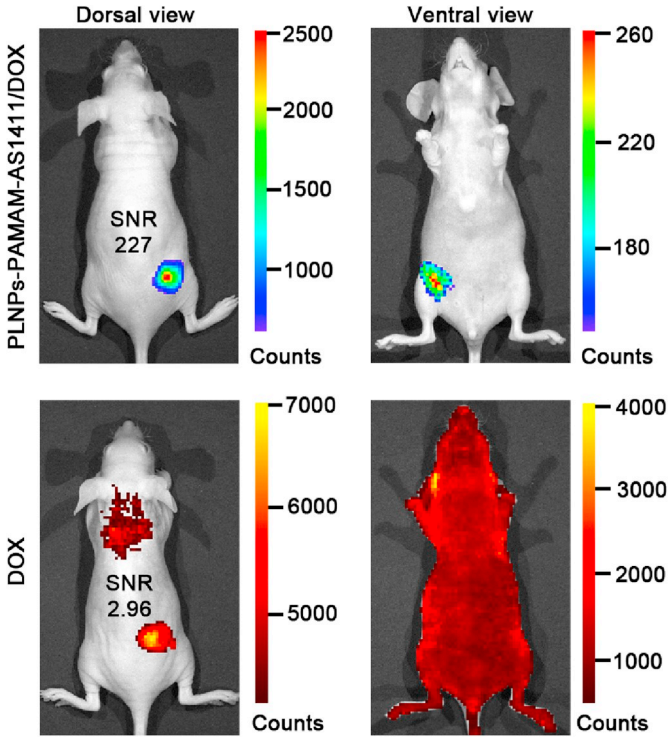

Fig. 6. *In vivo* imaging comparison of PLNPs and DOX after subcutaneous injection of PLNPs-PAMAM-AS1411/DOX and DOX. PLNPs-PAMAM-AS1411/DOX was irradiated with a 254 nm UV light for 5 min before injection, and the signal of PLNPs was acquired under the luminescent imaging mode without excitation. The signal of DOX was acquired in the fluorescent imaging mode with excitation at 500 nm.

This result indicates that AS1411 aptamer-guided tumor-targeting is feasible to enhance the inhibitory effect of the theranostic nanoprobe. In addition, free DOX gave the highest cytotoxicity because the DOX in the medium can rapidly diffuse into the nucleus to inhibit the DNA replication, which means that free DOX is not specific in the course of administration and possesses strong side effects on normal cells and tissues [18].

3.8. Chemotherapy

In vivo chemotherapy was conducted on HeLa tumor-bearing athymic nude mice to evaluate the therapeutic effect of PLNPs-PAMAM-AS1411/DOX. The mice were randomly divided into four groups: three treatment groups injected intravenously with free DOX, PLNPs-PAMAM-DOX and PLNPs-PAMAM-AS1411/DOX, respectively, and one control group injected with PBS only. As shown in Fig. 9a, the tumor growth of the control group was rapid and the tumor volume increased to about 9.5-fold of the initial volume after 20 days. In contrast, the three drug treatment groups all showed inhibition on tumor growth to some extents. However, the mice treated with PLNPs-PAMAM-AS1411/DOX exhibited dramatic therapeutic effect and the tumor inhibition rate can reach about 66% at 20 days after treatment (Fig. 9b), indicating that the nanovector with targeting and acid responsive drug delivery could maximize the antitumor efficiency. The tumor weights at 20 days after treatment are shown in Fig. 9c to further illustrate the good antitumor efficacy of PLNPs-PAMAM-AS1411/DOX *in vivo*. In addition, no appreciable change in the mice weight was observed in all groups throughout the treatment period (Fig. 9d), demonstrating the limited side effects of the PLNPs-PAMAM-AS1411/DOX.

4. Conclusions

In summary, we have shown the design, preparation, and application of the PAMAM dendrimer grafted persistent luminescent nanoplatform with the dual function of targeting and drug delivery for *in vitro* and *in vivo* imaging and chemotherapy. The synergistic effect of the renewable long NIR persistent luminescence from PLNPs, the specificity and affinity of aptamer AS1411 toward tumour cells, and the intracellular controlled release of DOX via a pH-sensitive hydrazone makes the PLNPs-PAMAM-AS1411/DOX full of potential for bioimaging and treatment of tumors with high specificity and efficiency. This work furnishes a prospective strategy to design the intelligent multifunctional nano-drug delivery systems for precise cancer theranostics.

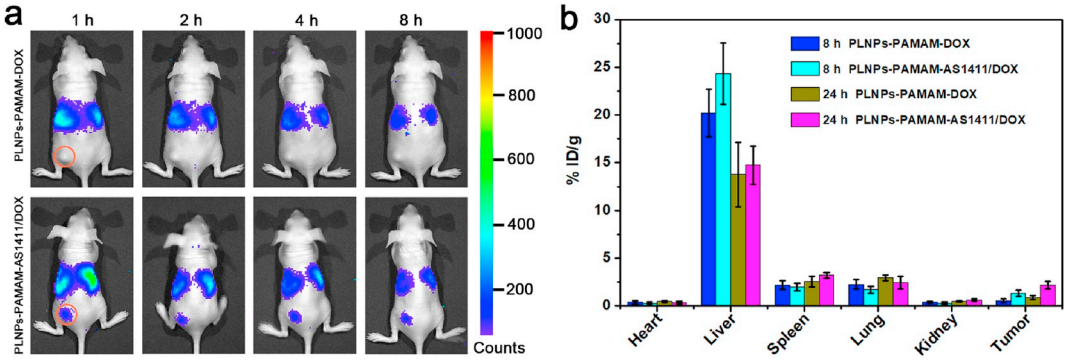

Fig. 7. (a) *In vivo* persistence luminescence images of HeLa tumor-bearing mice post intravenous injection of PLNPs-PAMAM-DOX and PLNPs-PAMAM-AS1411/DOX (irradiated with a 254 nm UV lamp before injection, irradiated with a 650 nm LED light for 2 min before each acquisition, circle represents tumor site). (b) Biodistributions of PLNPs-PAMAM-DOX and PLNPs-PAMAM-AS1411/DOX in HeLa tumor-bearing mice at 8 and 24 h after intravenous injection.

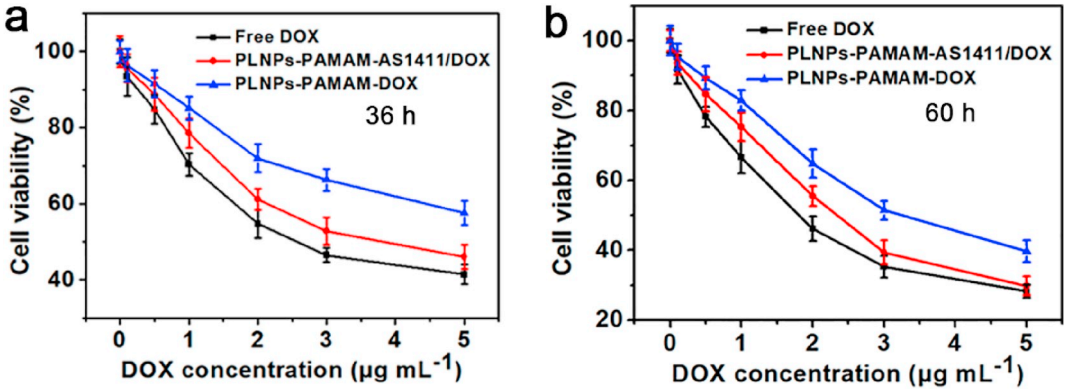

Fig. 8. Viability of HeLa cells in different mediums containing free DOX, PLNPs-PAMAM-AS1411/DOX and PLNPs-PAMAM-DOX with the same concentration of DOX in different periods: (a) 36 h; (b) 60 h.

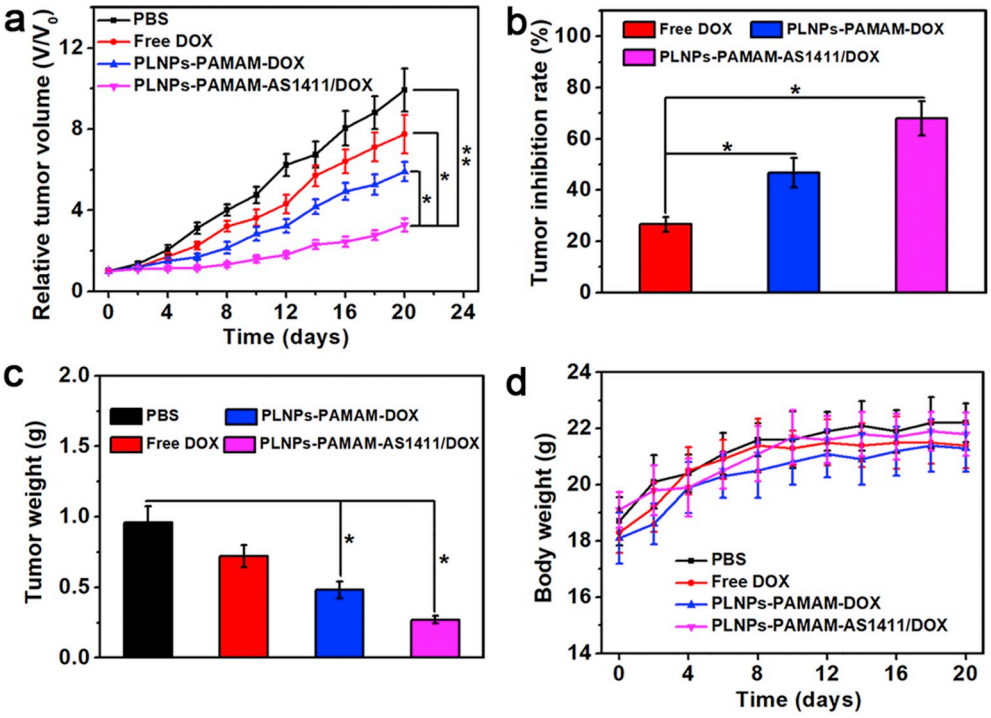

Fig. 9. (a) HeLa tumor growth profiles of mice treated with PBS, free DOX, PLNPs-PAMAM-DOX and PLNPs-PAMAM-AS1411/DOX. (b) Tumor growth inhibition ratio after 20 days treatment. (c) Tumor weights after different treatments. (d) Body weight changes of HeLa tumor-bearing mice treated with PBS, free DOX, PLNPs-PAMAM-DOX and PLNPs-PAMAM-AS1411/DOX.

CRediT authorship contribution statement

Hong-Jiao Zhang: Methodology, Investigation, Data curation, Writing - original draft. **Xu Zhao:** Methodology, Funding acquisition. **Li-Jian Chen:** Methodology, Funding acquisition. **Cheng-Xiong Yang:** Data curation. **Xiu-Ping Yan:** Conceptualization, Supervision, Writing - review & editing, Funding acquisition.

Acknowledgments

This work was supported by the National Natural Science Foundation of China (No. 21934002, 21804056 and 21804057), the China Postdoctoral Science Foundation (No. 2018M630511 and 2018M630509), and the Natural Science Foundation of Jiangsu Province, China (No. BK20180581 and BK20180584), the National First-class Discipline Program of Food Science and Technology (No. JUFSTR20180301) and the Fundamental Research Funds for the Central Universities (No. JUSRP51714B and JUSRP11846).

Appendix A. Supplementary data

Supplementary data to this article can be found online at https://doi.org/10.1016/j.talanta.2020.121209.

Notes

The authors declare no competing financial interest.

References

[1] R.L. Siegel, K.D. Miller, A. Jemal, Cancer statistics, CA-Cancer, J. Clin. 69 (2019) 7–34.
[2] R.L. Siegel, K.D. Miller, A. Jemal, Cancer statistics, CA-Cancer, J. Clin. 70 (2020) 7–30.
[3] D. Peer, J.M. Karp, S. Hong, O.C. Farokhzad, R. Margalit, R. Langer, Nanocarriers as an emerging platform for cancer therapy, Nat. Nanotechnol. 2 (2007) 751–760.
[4] T. Sun, Y.S. Zhang, B. Pang, D.C. Hyun, M. Yang, Y. Xia, Engineered nanoparticles for drug delivery in cancer therapy, Angew. Chem. Int. Ed. 53 (2014) 12320–12364.
[5] V.P. Torchilin, Multifunctional, stimuli-sensitive nanoparticulate systems for drug delivery, Nat. Rev. Drug Discov. 13 (2014) 813–827.
[6] W. Chen, J. Ouyang, H. Liu, M. Chen, K. Zeng, J. Sheng, Z. Liu, Y. Han, L. Wang, J. Li, L. Deng, Y.N. Liu, S. Guo, Black phosphorus nanosheet-based drug delivery system for synergistic photodynamic/photothermal/chemotherapy of cancer, Adv. Mater. 29 (2017) 1603864.
[7] M.E. Caldorera-Moore, W.B. Liechty, N.A. Peppas, Responsive theranostic systems: integration of diagnostic imaging agents and responsive controlled release drug delivery carriers, Acc. Chem. Res. 44 (2011) 1061–1070.
[8] Q.M. de Chermont, C. Chanéac, J. Seguin, F. Pellé, S. Maîtrejean, J.-P. Jolivet, D. Gourier, M. Bessodes, D. Scherman, Nanoprobes with near-infrared persistent luminescence for *in vivo* imaging, Proc. Natl. Acad. Sci. U.S.A. 104 (2007) 9266–9271.
[9] S.-K. Sun, H.-F. Wang, X.-P. Yan, Engineering persistent luminescence nanoparticles for biological applications: from biosensing/bioimaging to theranostics, Acc. Chem. Res. 51 (2018) 1131–1143.
[10] A. Abdukayum, J.T. Chen, Q. Zhao, X.P. Yan, Functional near infrared-emitting Cr^{3+}/Pr^{3+} co-doped zinc gallogermanate persistent luminescent nanoparticles with superlong afterglow for *in vivo* targeted bioimaging, J. Am. Chem. Soc. 135 (2013) 14125–14133.
[11] Y.-J. Li, X.-P. Yan, Synthesis of functionalized triple-doped zinc gallogermanate nanoparticles with superlong near-infrared persistent luminescence for long-term oral administrated bioimaging, Nanoscale 8 (2016) 14965–14970.
[12] H.-J. Zhang, X. Zhao, L.-J. Chen, C.-X. Yang, X.-P. Yan, pH-driven targeting nanoprobe with dual-responsive drug release for persistent luminescence imaging and chemotherapy of tumor, Anal. Chem. 92 (2020) 1179–1188.
[13] Y.-J. Li, C.-X. Yang, X.-P. Yan, Biomimetic persistent luminescent nanoplatform for autofluorescence-free metastasis tracking and chemophotodynamic therapy, Anal. Chem. 90 (2018) 4188–4195.
[14] L.-J. Chen, C.-X. Yang, X.-P. Yan, Liposome-coated persistent luminescence nanoparticles as luminescence trackable drug carrier for chemotherapy, Anal. Chem. 89 (2017) 6936–6939.
[15] Y. Lv, D. Ding, Y. Zhuang, Y. Feng, J. Shi, H. Zhang, T.L. Zhou, H. Chen, R.J. Xie, Chromium-doped zinc gallogermanate@zeolitic imidazolate framework-8: a multifunctional nanoplatform for rechargeable *in vivo* persistent luminescence imaging and pH-responsive drug release, ACS Appl. Mater. Interfaces 11 (2019) 1907–1916.
[16] J.M. Frechet, Functional polymers and dendrimers: reactivity, molecular architecture, and interfacial energy, Science 263 (1994) 1710–1715.
[17] J. Khandare, M. Calderon, N.M. Dagia, R. Haag, Multifunctional dendritic polymers in nanomedicine: opportunities and challenges, Chem. Soc. Rev. 41 (2012) 2824–2848.
[18] Y. Pu, S. Chang, H. Yuan, G. Wang, B. He, Z. Gu, The anti-tumor efficiency of poly (L-glutamic acid) dendrimers with polyhedral oligomeric silsesquioxane cores, Biomaterials 34 (2013) 3658–3666.
[19] S. Mignani, J. Rodrigues, H. Tomas, M. Zablocka, X. Shi, A.M. Caminade, J.P. Majoral, Dendrimers in combination with natural products and analogues as anti-cancer agents, Chem. Soc. Rev. 47 (2018) 514–532.
[20] S. Yue, X. Song, W. Song, S. Bi, An enzyme-free molecular catalytic device: dynamically self-assembled DNA dendrimers for in situ imaging of microRNAs in live cells, Chem. Sci. 10 (2019) 1651–1658.
[21] T. Wei, C. Chen, J. Liu, C. Liu, P. Posocco, X. Liu, Q. Cheng, S. Huo, Z. Liang, M. Fermeglia, S. Pricl, X.J. Liang, P. Rocchi, L. Peng, Anticancer drug nanomicelles formed by self-assembling amphiphilic dendrimer to combat cancer drug resistance, Proc. Natl. Acad. Sci. U.S.A. 112 (2015) 2978–2983.
[22] P. Lai, P. Lou, C. Peng, C. Pai, W. Yen, M. Huang, T. Young, M. Shieh, Doxorubicin delivery by polyamidoamine dendrimer conjugation and photochemical internalization for cancer therapy, J. Contr. Release 122 (2007) 39–46.
[23] S. Nigam, D. Bahadur, Dendrimer-conjugated iron oxide nanoparticles as stimuli-responsive drug carriers for thermally-activated chemotherapy of cancer, Colloids Surf. B 155 (2017) 182–192.
[24] C.C. Lee, J.A. Mackay, J.M. Frechet, F.C. Szoka, Designing dendrimers for biological applications, Nat. Biotechnol. 23 (2005) 1517–1526.
[25] D. Zhong, H. Wu, Y. Wu, Y. Li, X. Xu, J. Yang, Z. Gu, Rational design and facile fabrication of biocompatible triple responsive dendrimeric nanocages for targeted drug delivery, Nanoscale 11 (2019) 15091–15103.
[26] Y. Fan, J. Zhang, M. Shi, D. Li, C. Lu, X. Cao, C. Peng, S. Mignani, J.P. Majoral, X. Shi, Poly (amidoamine) dendrimer-coordinated copper (II) complexes as a theranostic nanoplatform for the radiotherapy-enhanced magnetic resonance imaging and chemotherapy of tumors and tumor metastasis, Nano Lett. 19 (2019) 1216–1226.
[27] M. Han, M.Y. Huang-Fu, W.W. Guo, N.N. Guo, J. Chen, H.N. Liu, Z.Q. Xie, M.T. Lin, Q.C. Wei, J.Q. Gao, MMP-2-sensitive HA end-conjugated poly (amidoamine) dendrimers via click reaction to enhance drug penetration into solid tumor, ACS Appl. Mater. Interfaces 9 (2017) 42459–42470.
[28] X.L. Guo, X.X. Kang, Y.Q. Wang, X.J. Zhang, C.J. Li, Y. Liu, L.B. Du, Co-delivery of cisplatin and doxorubicin by covalently conjugating with polyamidoamine dendrimer for enhanced synergistic cancer therapy, Acta Biomater. 84 (2019) 367–377.
[29] W. Cheng, J. Nie, L. Xu, C. Liang, Y. Peng, G. Liu, T. Wang, L. Mei, L. Huang, X. Zeng, pH-sensitive delivery vehicle based on folic acid-conjugated polydopamine-modified mesoporous silica nanoparticles for targeted cancer therapy, ACS Appl. Mater. Interfaces 9 (2017) 18462–18473.
[30] S.H. Park, J.H. Zheng, V.H. Nguyen, S.N. Jiang, D.Y. Kim, M. Szardenings, J.H. Min, Y. Hong, H.E. Choy, J.J. Min, RGD Peptide cell-surface display enhances the targeting and therapeutic efficacy of attenuated salmonella-mediated cancer therapy, Theranostics 6 (2016) 1672–1682.
[31] X. Liu, W. Shao, Y. Zheng, C. Yao, L. Peng, D. Zhang, X.Y. Hu, L. Wang, GSH-responsive supramolecular nanoparticles constructed by β-d-galactose-modified pillar [5] arene and camptothecin prodrug for targeted anticancer drug delivery, Chem. Commun. 53 (2017) 8596–8599.
[32] D. Zhao, J.Q. Xu, X.Q. Yi, Q. Zhang, S.X. Cheng, R.X. Zhuo, F. Li, pH-activated targeting drug delivery system based on the selective binding of phenylboronic acid, ACS Appl. Mater. Interfaces 8 (2016) 14845–14854.
[33] G. Zhou, O. Latchoumanin, L. Hebbard, W. Duan, C. Liddle, J. George, L. Qiao, Aptamers as targeting ligands and therapeutic molecules for overcoming drug resistance in cancers, Adv. Drug Deliv. Rev. 134 (2018) 107–121.
[34] A. Pusuluri, V. Krishnan, V. Lensch, A. Sarode, E. Bunyan, D.R. Vogus, S. Menegatti, H.T. Soh, S. Mitragotri, Treating tumors at low drug doses using an aptamer-peptide synergistic drug conjugate, Angew. Chem. Int. Ed. 58 (2019) 1437–1441.
[35] P. Zhang, F. Cheng, R. Zhou, J. Cao, J. Li, C. Burda, Q. Min, J.J. Zhu, DNA-hybrid-gated multifunctional mesoporous silica nanocarriers for dual-targeted and microRNA-responsive controlled drug delivery, Angew. Chem. Int. Ed. 53 (2014) 2371–2375.
[36] R. Savla, O. Taratula, O. Garbuzenko, T. Minko, Tumor targeted quantum dot-mucin 1 aptamer-doxorubicin conjugate for imaging and treatment of cancer, J. Contr. Release 153 (2011) 16–22.
[37] A. Van Driessche, A. Kocere, H. Everaert, L. Nuhn, S. Van Herck, G. Griffiths, F. Fenaroli, B.G. De Geest, pH-sensitive hydrazone-linked doxorubicin nanogels via polymeric-activated ester scaffolds: synthesis, assembly, and *in vitro* and *in vivo* evaluation in tumor-bearing zebrafish, Chem. Mater. 30 (2018) 8587–8596.
[38] B. Ma, W. Zhuang, Y. Wang, R. Luo, Y. Wang, pH-sensitive doxorubicin-conjugated prodrug micelles with charge-conversion for cancer therapy, Acta Biomater. 70 (2018) 186–196.
[39] X.L. Xu, K.J. Lu, M.L. Zhu, Y.L. Du, Y.F. Zhu, N.N. Zhang, X.J. Wang, X.Q. Kang, D.M. Xu, X.Y. Ying, R.S. Yu, C.Y. Lu, J.S. Ji, J. You, Y.Z. Du, Sialic acid-functionalized pH-triggered micelles for enhanced tumor tissue accumulation and active cellular internalization of orthotopic hepatocarcinoma, ACS Appl. Mater. Interfaces 10 (2018) 31903–31914.
[40] D. Dheer, J. Nicolas, R. Shankar, Cathepsin-sensitive nanoscale drug delivery systems for cancer therapy and other diseases, Adv. Drug Deliv. Rev. 151–152 (2019) 130–151.

[41] J. Mu, J. Lin, P. Huang, X. Chen, Development of endogenous enzyme-responsive nanomaterials for theranostics, Chem. Soc. Rev. 47 (2018) 5554–5573.
[42] M. Shahriari, M. Zahiri, K. Abnous, S.M. Taghdisi, M. Ramezani, M. Alibolandi, Enzyme responsive drug delivery systems in cancer treatment, J. Contr. Release 308 (2019) 172–189.
[43] A. Pourjavadi, S.H. Hosseini, M. Alizadeh, C. Bennett, Synthesis of new electromagnetic nanocomposite based on modified Fe_3O_4 nanoparticles with enhanced magnetic, conductive, and catalytic properties, Colloids Surf., B 116 (2014) 49–54.
[44] M.M. Tomayko, C.P. Reynolds, Determination of subcutaneous tumor size in athymic (nude) mice, Canc. Chemother. Pharmacol. 24 (1989) 148–154.
[45] D.M. Euhus, C. Hudd, M.C. Laregina, F.E. Johnson, Tumor measurement in the nude mouse, J. Surg. Oncol. 31 (1986) 229–234.